A Novel Approach To Prepare Poly(3,4-ethylenedioxythiophene) Nanoribbons between V_2O_5 Layers by Microwave Irradiation

A. Vadivel Murugan,*,† C. W. Kwon,‡ G. Campet,‡ B. B. Kale,† A. B. Mandale,§ S. R. Sainker,§ Chinnakonda S. Gopinath,§ and K. Vijayamohanan*,§

Centre for Materials for Electronics Technology (C-MET), Department of Information Technology, Government of India, Dr. Homibhabha Road, Panchawati, Pune-411008, India, Institut de Chimie de la Matière Condensée de Bordeaux (ICMCB), CNRS 87, Avenue du Dr. A Schweitzer, 33608 Pessac, France, and National Chemical Laboratory, Dr. Homi Bhabha Road, Pune-411008, India

Received: March 15, 2004; In Final Form: May 27, 2004

Rapid synthesis of poly(3,4-ethylenedioxythiophene) (PEDOT) nanoribbons interleaved between the layers of crystalline V_2O_5 is achieved for the first time under microwave irradiation via the redox intercalative polymerization reaction of 3,4-ethylenedioxythiophene (EDOT) monomer and crystalline V_2O_5 at different time intervals. Compared with the conventional 12 h of refluxing for intercalative polymerization, the microwave-assisted redox polymerization process proceedes rapidly, enabling the expansion of the interlayer spacing of crystalline V_2O_5 from 0.43 to 1.41 nm within 8 min. The characterization of this material using powder XRD, XPS, EPR, SEM, and HRTEM analysis supports the intercalation of the polymer between V_2O_5 layers, leading to enhanced bidimensionality. XPS analysis clearly shows the presence of mixed-valent V^{4+}/V^{5+} in the V_2O_5 framework after the redox intercalative polymerization, which also confirms charge transfer from the polymer to the V_2O_5 framework. EPR study also reveals redox processes during EDOT insertion and polymerization between the V_2O_5 layers. After PEDOT insertion into V_2O_5, the EPR signal from VO^{2+} is more pronounced as the intensity of the signal increases as compared to that of pristine V_2O_5. This nanocomposite when coupled with a large-area Li foil electrode in 1 M $LiClO_4$ in a mixture of ethylene and dimethyl carbonate (1:1 by volume) gives a discharge capacity of ∼350 mA h g^{-1}, which is significantly higher than that of pristine V_2O_5.

Introduction

Recently, nanoscale building blocks, such as nanotubes, nanowires, and nanoribbons, have attracted extensive interest because of their size and shape-dependent properties, enabling to them to be tuned for a wide range of applications.[1−5] Indeed, significant progress in "nanochemistry" has given birth to a newly emerging area of materials, called "nanohybrid" or "nanocomposite" materials, which results from the tuning of molecular level interactions of dissimilar organic and inorganic components to form new unique functional materials with improved properties. This approach has been successfully used recently for the synthesis of novel nanocomposite materials by a redox intercalation strategy to prepare hybrid 2D lamellar transition-metal oxides having enhanced synergic activity.[6−19] It is well-known that intercalation leads to changes in the interlayer spacing for layered materials.[11] For example, several conducting polymers such as polyaniline, polypyrrole, and polythiophene are known to oxidatively polymerize when intercalated into highly oxidizing transition-metal oxides such as V_2O_5.[6−19] Indeed, the field has expanded in such a way that several recent reports focus only on specific preparation of conducting polymer nanocomposites and their functional properties particularly on the possibility of enhancing the energy storage characteristics for lithium batteries.[11−19] However, the preparation of many of these hybrid nanocomposite materials often involves lengthy procedures with several steps and needs more time before the formation of the hybrid nanocomposite. It is, therefore, necessary to develop more efficient methods of synthesis involving simplified preparation procedures and short time, and the use of microwave-assisted synthesis is especially important in this regard. Consequently, the use of microwave irradiation for the synthesis of inorganic materials has gained greater importance in recent years.[20,21] The method offers several advantages over conventional routes, the most important of them being cleanliness, short reaction times, and energy economy.[20−24] This efficient method of microwave-irradiated synthesis has been reported to lead to an increase in reaction rates and improvement of the product formation.[20−22]

Recently, we have demonstrated the preliminary studies of conducting poly(3,4-ethylenedioxythiophene) based nanocomposite cathode material for lithium batteries by a conventional method.[14,16−18] In comparison, here we report an ecofriendly and rapid microwave-assisted synthesis and characterization of organic−inorganic PEDOT/V_2O_5 nanocomposites, where PEDOT forms nanoribbons in the interlayer spacing. The primary objective is to understand the microwave-irradiated redox intercalation reaction of EDOT with V_2O_5 powder and the subsequent polymerization. These observations are supported by several physicochemical data including the microstructure of the PEDOT/V_2O_5 nanocomposite during the polymer nanoribbon formation between the V_2O_5 layers. To our knowledge, this is the first study of microwave-assisted preparation of PEDOT/V_2O_5 nanocomposites, and the usefulness of this hybrid

* To whom correspondence should be addressed. E-mail: vadivel12@hotmail.com (A.V.M.); viji@ems.ncl.res.in (K.V.).
† Government of India.
‡ ICMCB.
§ National Chemical Laboratory.

10.1021/jp048859g CCC: $27.50
Published on Web 06/29/2004

material as a high-energy-density cathode for lithium batteries has been demonstrated in comparison with pristine V_2O_5.

Experimental Section

Materials. Vanadium pentoxide (99.9%), lithium metal foil (99.9%), $LiClO_4$ (99.99%), poly(tetrafluoroethylene) (PTFE; 99.99%), propylene carbonate (PC; 99.9%), and dimethyl carbonate (DMC; 99%) from Aldrich were used without further purification. 3,4-Ethylenedioxythiophene (EDOT; Bayer AG Germany) was distilled under vacuum prior to use. Ethylene carbonate (EC; Prolabo, 99%) and ketjenblack were used as received. All experiments were conducted with deionized water.

Characterization. The powder X-ray diffraction analysis was carried out using a Rigaku X-ray diffractometer (Rigaku miniflex) equipped with Ni-filtered Cu Kα (1.542 Å) radiation and a graphite crystal monochromator. X-ray photoelectron spectroscopy (XPS) was carried out on a VG Microtech Multilab ESCA 3000 spectrometer using a nonmonochromatized Al Kα X-ray source ($h\nu = 1486.6$ eV). The base pressure in the analysis chamber was maintained in the 10^{-10} Torr range. The energy resolution of the spectrometer was set at 1.1 eV with Al Kα radiation at a pass energy of 50 eV. Binding energy (BE) calibration was performed with the Au $4f_{7/2}$ core level at 83.9 eV. The error in all the BE values reported here is within ±0.1 eV. The EPR spectra were registered as the first derivative of the absorption signal with an ERS-220/Q spectrometer (ex-GDR) within the temperature range between 85 K and room temperature. The *g* factors were established with respect to a Mn^{2+}/ZnS standard. The signal intensity was determined by double integration of the experimental EPR spectrum. Recordings at different microwave powers were used to distinguish the EPR signals. Electronic conductivity measurements were made on compaction of powder in pellet form by using a four-point probe conductivity method. Scanning electron microscopy (SEM) was carried out with a Philips XL-30 microscope at an accelerating voltage of 20 kV after the samples were mounted onto Al stubs with gold coatings. For TEM imaging (TEM model JEM-2010, JEOL) the powder was first dispersed in ethanol by ultrasonication, and then the suspension was drop casted once copper grid coated with carbon films and dried. Elemental analysis was carried out using inductively coupled plasma optical emission spectroscopy (ICP-OES; Perkin-Elmer, 1000) and using a CE-Instruments-EA-1110 CHNO-S analyzer.

Microwave-Assisted Synthesis of Nanocomposites. The mixtures of V_2O_5 (1.1 mM) and EDOT monomer (0.42 mM) in doubly distilled water were treated in a double-walled Teflon-lined digestion vessel and placed on a turntable for uniform heating using a microwave digestion system (MLS-120 Mega, GmbH, Germany). The outer shell of the reaction vessel was composed of a high-strength polymer called Ultem polyetherimide, and the inner liner was composed of Teflon. These vessels were transparent to microwave radiation, and hence, the contents in these vessels could be heated hydrothermally. When the reaction mixture was exposed to microwave radiation, the microwaves induced rotation of the dipoles within the liquid, forcing the polar molecules to align and relax in the field of oscillating electromagnetic radiations, causing the liquid to become hot. Thus, the heat produced within the liquid is not transferred from the vessel as in other conventional systems. Computer-controlled microwave-hydrothermal treatments were conducted for different durations using 2.45 GHz microwave radiation with full power (950 W). After the microwave irradiation, the solid was filtered off and washed repeatedly with water and ethanol, and the dark blue-black powder was dried in air. Elemental analysis of the nanocomposite prepared by a direct microwave irradiation after 8 min intervals is as follows. $(C_6H_4O_2S)_{0.026}\cdot V_2O_5$: C, 0.86; H, 1.13; S, 0.18; V, 43.96.

Electrochemical Measurements. The electrochemical measurements were performed using a button-type cell configuration with the aid of a computer-controlled PGS201T (Tacussel) potentiostat/galvanostat system. The oxidized composite cathodes were made by intimately mixing 70% (by weight) active material, 25% Ketjenblack, and 5% PTFE. The surface area of electrodes and weight of the active material were adjusted to ~1 cm^2 and ~20 mg, respectively, for reproducibility. These electrodes were dried under vacuum at ~80 °C for more than 3 h, and introduced into an argon-filled glovebox without any exposure to air. The electrolyte was 1 M $LiClO_4$ in a 1:1 mixture (by volume) of EC/DMC, and a lithium foil was used as an anode. For charge/discharge experiments, a constant current of 15 mA/g was applied between 2.0 and 4.4 V (vs Li^+/Li). For cyclic voltammetry, the voltage was cycled between 2.2 and 3.8 V at a sweep rate of 0.5 mV s^{-1}.

Results and Discussion

X-ray Diffraction Studies. Figure 1 shows X-ray diffraction patterns of conducting polymer based PEDOT/V_2O_5 nanocomposites synthesized by the direct in situ oxidation of 3,4-ethylenedioxythiophene monomer into crystalline V_2O_5 using microwave irradiation at different intervals. The characteristic broad *d*(001) peak of the nanocomposite can be observed around a 2θ value of 6.24°, although sharp peaks attributed to crystalline V_2O_5 also appear. However, the intensity of the above low-angle *d*(001) reflection increases with increasing microwave irradiation time (Figure 1 inset). On the other hand, the *d*(200) and *d*(101) reflections are diffused with increasing reaction time. The expansion of the interlayer *d*(001) spacing of V_2O_5 increases linearly from 0.43 to 1.41 nm with an increase in irradiation time. For example, when the microwave irradiation time is short (5−7 min), two phases of nanocomposite and unreacted crystalline V_2O_5 are evident in the XRD pattern, and the color of the products is yellow-green during the course of reaction, which is characteristic of V_2O_5 containing pentavalent vanadium (V^{5+}). After the microwave irradiation of the mixture for 7.5−8 min, the intensity (I/I_0) of the *d*(001) line increases to a maximum corresponding to the nanocomposite formation, and interestingly the color of the product completely changes to blue-black. These results are listed in Table 1 along with a comparison of the spacings calculated from lattice constants and electronic conductivities of nanocomposites. The *d*(001) spacing is larger than those for pure V_2O_5 although there are minor changes with the nature of the incorporated polymer. Interestingly, the values of the *d*(110) and *d*(400) spacings, perpendicular to the *c* axis, are the same for all vanadium bronzes, polymer/vanadium composites, and also pure V_2O_5.[25,26] The strongest peak observed at the low angle corresponding to the (001) plane of the layered V_2O_5 structure is directly related to the interlayer spacing. Thus, the main features of the V_2O_5 diffraction patterns in the composites are clearly modified by the appearance of a sharp diffused scattering feature and an increase in the intensity of the (001) peak. These results are in excellent agreement with the X-ray diffraction patterns of the polyaniline/V_2O_5 nanocomposite reported by Huguenin et al.[15]

Electron Microscopy (SEM/HRTEM). A comparison of the SEM images of the PEDOT/V_2O_5 nanocomposite synthesized by the direct microwave irradiation at 8 min intervals and crystalline V_2O_5 is illustrated in Figure 2a,b. It is apparent that PEDOT/V_2O_5 composites form a continuous and relatively

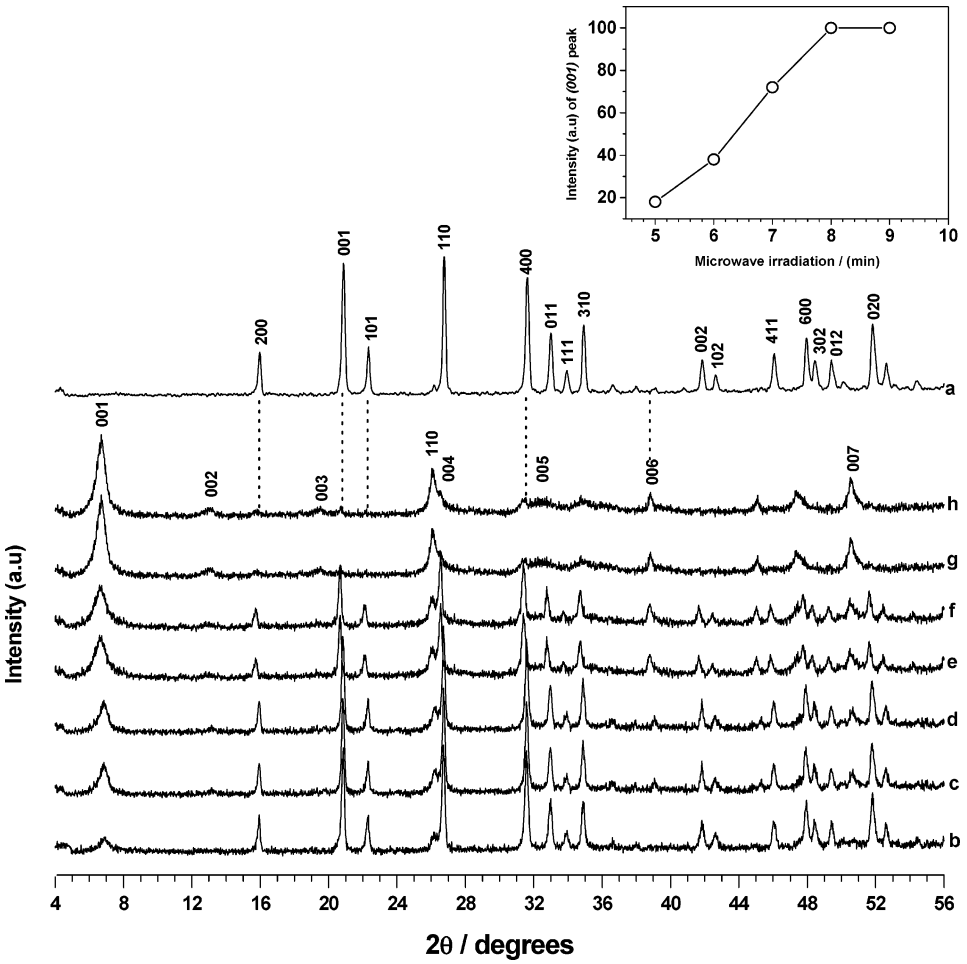

Figure 1. Powder XRD pattern of the (a) crystalline V_2O_5 and PEDOT/V_2O_5 nanocomposite synthesized by a direct microwave irradiation at different intervals such as (b) 5.0 min, (c) 5.5 min, (d) 6.0 min, (e) 6.5 min, (f) 7.0 min, (g) 7.5 min, and (h) 8.0 min. The inset figure shows the intensity of the (001) peak vs microwave irradiation time of the PEDOT/V_2O_5 nanocomposite formation at different intervals.

TABLE 1: Interlayer Spacing (nm) for V_2O_5 and the PEDOT/V_2O_5 Nanocomposites Prepared Using Microwave Irradiation at Different Intervals of Time

sample[a]	microwave irradiation time (min)	2θ(001) (deg)	*d*(*hkl*) (nm)			electronic conductivity, σ (S cm^{-1})
			d(001)	*d*(110)	*d*(400)	
V_2O_5		20.40	0.435	0.338	0.286	6.78×10^{-5}
VP-5.0	5.0	6.40	1.379	0.390	0.287	8.43×10^{-5}
VP-5.5	5.5	6.39	1.379	0.390	0.287	2.24×10^{-4}
VP-6.0	6.0	6.38	1.384	0.391	0.287	2.65×10^{-4}
VP-6.5	6.5	6.37	1.385	0.391	0.287	5.49×10^{-4}
VP-7.0	7.0	6.26	1.410	0.347	0.288	8.72×10^{-4}
VP-7.5	7.5	6.25	1.412	0.347	0.288	3.26×10^{-3}
VP-8.0	8.0	6.24	1.415	0.347	0.289	4.46×10^{-3}

[a] VP = PEDOT/V_2O_5 nanocomposite. The number following the hyphen indicates the irradiation time (min).

homogeneous matrix with a clear lamellar morphology after 8 min of microwave irradiation. The incorporation of PEDOT into the V_2O_5 host accompanies morphological changes in agreement with the results of XRD patterns, but can be seen only at high resolution. In addition, the SEM micrographs also suggest that there is no bulk deposition of the polymer on the surface of the microcrystallites. More significantly, the high-resolution transmission electron microscopy (HRTEM) image shows nanoribbon morphology of the microwave-irradiated PEDOT/V_2O_5 nanocomposite (8 min), as illustrated in Figure 2c, thus suggesting that the in situ redox intercalative polymerization by microwave irradiation is topotactic and the structure of the host still remains unchanged. As can be seen from the HRTEM image, the V_2O_5 host consists of several conducting polymer nanoribbons and the low scattering power causes bright contrast for white lines, each ~1.4 nm between two dark fringes of vanadate layers. The same ribbon thickness of about 1.41 nm can be evaluated from the most pronounced intensity maximum found in the broad X-ray diffraction pattern *d*(001) (Figure 1g). Thus, from the HRTEM image of the nanocomposite material, we conclude that highly crystalline vanadium oxide is separated by alternating organic conducting polymer nanoribbons in this hybrid material. This type of structure of the V_2O_5/PEDOT nanocomposite can be well described (Scheme 1) as a stack of long ribbon-like slabs which are an assembly of well-defined bilayers of single V_2O_5 layers made of square-pyramidal VO_5 units with PEDOT nanoribbons residing between them. The distance of closest approach between the bilayers is approximately 1.4 nm. This is in good agreement with the recent proposition of Petkov et al.,[27] where a chain-based slab structure

SCHEME 1. Structure of V_2O_5 Slabs[a]

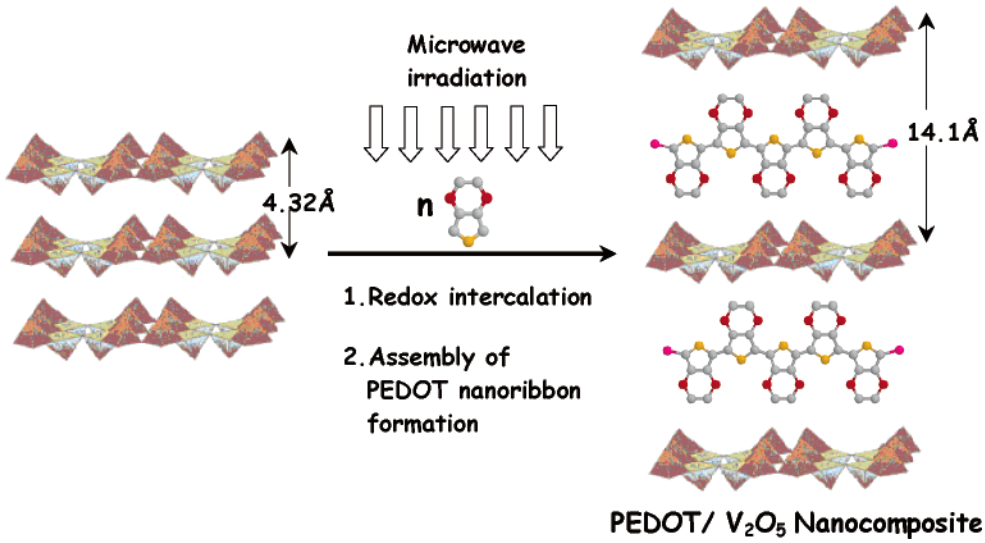

[a] Each V_2O_5 (polyhedron model) single layer is made up of square-pyramidal VO_5 units, showing PEDOT nanoribbons (ball-and-stick model) interleaved between V_2O_5 chains as also supported by the HRTEM image.

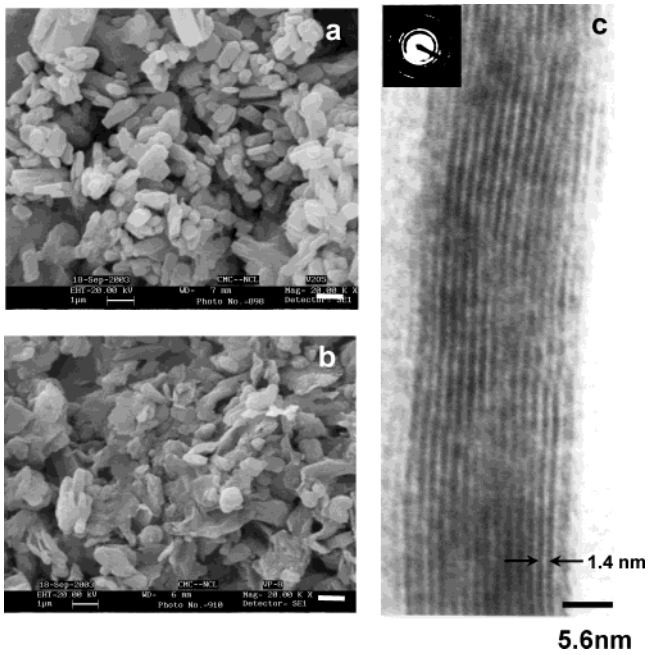

Figure 2. SEM images of (a) V_2O_5 and (b) the PEDOT/V_2O_5 nanocomposite synthesized by a direct microwave irradiation for 8 min and (c) HRTEM image of PEDOT nanoribbons intercalated into V_2O_5 layers to form a nanocomposite. The scale bars indicated on the SEM images correspond to 1 μm.

is found to be responsible for the formation of long nanoribbons in both crystalline V_2O_5 and the $V_2O_5 \cdot nH_2O$ xerogel.

X-ray Photoelectron Spectroscopy. XPS is a surface-specific technique to study the polymer−V_2O_5 interaction and vanadium (V^{5+}/V^{4+}) oxidation state, after the redox polymer intercalation. XPS results from the V 2p and O 1s core levels of the polymer-intercalated nanocomposite are displayed in Figure 3. The spectra are presented after the removal of the O 1s X-ray satellite around 518−520 eV and after Shirley background subtraction. A low-BE feature is apparent along with V^{5+} species at 517.2 eV. Deconvolution of the V 2p core levels clearly shows the above low-BE feature at 515.7 eV, which is attributed to V^{4+}. The above BE values are in good correspondence with the standard compounds.[28] Using the deconvoluted peak area and

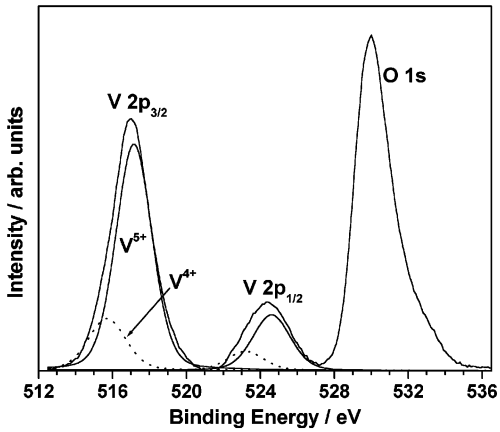

Figure 3. X-ray photoelectron spectra of the PEDOT/V_2O_5 nanocomposite prepared from direct microwave irradiation for 8 min.

the photoionization cross section of the V $2p_{3/2}$ level, the amount of V^{4+} is calculated to be 19% in total vanadium. This clearly indicates a charge transfer from the polymer to V_2O_5, indicating the effectiveness of the interaction between the polymer and V_2O_5. It is speculated here that the above interaction might be through the S atom of the polymer, as it is electron-rich; however, the above suggestion could not be confirmed since the S 2p signal is hardly seen in XPS, perhaps due to the low-photoionization cross section,[29] and further work is in progress with different amounts of polymer incorporation into V_2O_5.

Electron Paramagnetic Resonance (EPR) Spectroscopy. EPR spectroscopy is an excellent probe to study the nature of free spins in PEDOT/V_2O_5, since both the polymer and the reduced V_2O_5 framework are paramagnetic and hence EPR active. EPR study of PEDOT/V_2O_5 hybrids throws further light on the redox processes during EDOT insertion and polymerization between the V_2O_5 layers. Accordingly, Figure 4 compares the EPR spectra of PEDOT/V_2O_5 hybrids with that of V_2O_5. The EPR spectrum of V_2O_5 shows a single Lorentzian line with $g = 1.978$ and line widths varying between 13 and 15 mT, indicating the stoichiometry of V_2O_5 to be $V_2O_{5-\delta}$ or $V_{2+\epsilon}O_5$. On cooling, a weak fine structure superimposed on the Lorentzian line becomes more pronounced due to an impure vanadyl (VO^{2+}) species[30,31] which consists of a V^{4+} ion (d^1 configuration) and a close oxide shell, O^{2-}. The lack of well-resolved

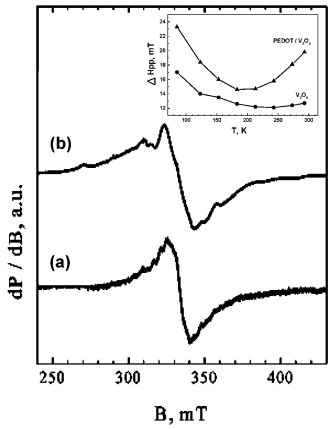

Figure 4. EPR spectra at 85 K of V_2O_5 and the PEDOT/V_2O_5 nanocomposite. The inset shows the corresponding temperature evolution of the EPR line width of nonisolated VO^{2+} complexes for (a) pristine V_2O_5, and (b) the PEDOT/V_2O_5 nanocomposite.

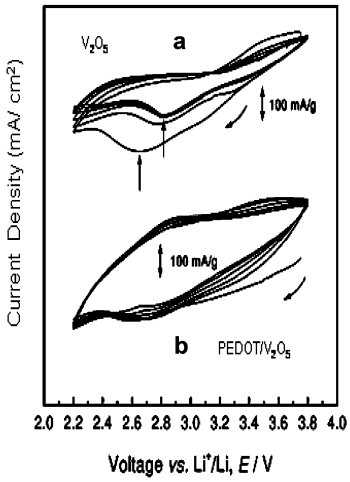

Figure 5. Cyclic voltammograms of (a) pristine V_2O_5 and (b) the PEDOT/V_2O_5 nanocomposite prepared from direct microwave irradiation for 8 min at 0.5 mV/s between 2.2 and 3.8 V vs Li^+/Li.

fine structure of the EPR spectrum of pristine V_2O_5 can be related to a nonisolated VO^{2+} species. This hints that the impure VO^{2+} species are located close to one to another, thus giving rise to dipole−dipole and exchange magnetic interactions between them. After EDOT insertion into V_2O_5, the EPR signal from VO^{2+} is more pronounced as the intensity of the signal increases about 200 times as compared to that of pristine V_2O_5. In addition, the signal intensity correlates well with the amount of the incorporated polymer; the relative intensity is 1.0 for the PEDOT/V_2O_5 composite sample. Irrespective of the strong increase in the signal intensity, a well-resolved fine structure is observed for the PEDOT/V_2O_5 sample (Figure 4). The fitting of the experimental spectrum enables differentiation of the two signals, the ratio between them being dependent on the recording temperature. At 85 K, there is a signal with tetragonally symmetric **g** and hyperfine tensors ($g_\perp = 1.9913$, $g_{||} = 1.9399$; $A_\perp = 66 \times 10^{-4}$; $A_{||} = 180 \times 10^{-4}$ cm^{-1}), as well as a single line with Lorentzian shape, $g = 1.983$, and $\Delta H_{pp} = 23.3$ mT. While the temperature is increased, the single Lorentzian accounts mainly for the EPR profile of PEDOT/V_2O_5. The two signals can be assigned to the isolated and nonisolated VO^{2+} complexes, respectively. The observed **g** and **A** tensors of isolated VO^{2+} in the PEDOT/V_2O_5 composite are close to those of VO^{2+} in $[VO(H_2O)_5]^{2+}$ ($g_\perp = 1.980$, 1.981, $g_{||} = 1.913$; $A_\perp = 71$, 72×10^{-4}, $A_{||} = 180 \times 10^{-4}$ cm^{-1}), indicating an ionic character of the bond between VO^{2+} and the equatorial ligands. The temperature evolution of the EPR line width is also observed for nonisolated VO^{2+} species in the PEDOT/V_2O_5 composite. The line width decreases on cooling from 293 to 183 K, passing through a minimum, and then increases interestingly again below 183 K (Figure 4 inset). However, the competition between dipole−dipole and exchange interactions may account for the observed differences in the line width of nonisolated VO^{2+} species. This clearly indicates differences in the distribution of VO^{2+} species, suggesting the role of PEDOT in controlling the distribution of VO^{2+}.

Electronic Conductivity. The electrical transport behavior of the nanocomposite can be understood by considering the insertion of poly(3,4-ethylenedioxythiophene) in V_2O_5 powder as a composite system in which two different types of low-dimensional electronic conductors coexist at the molecular level in a dimensionally constrained environment. Two types of charge carriers can be present in these materials, small polarons (electrons) associated with the d^1 (V^{4+}) centers on the vanadium oxide lattice and large polarons on the poly(3,4-ethylenedioxythiophene) backbone. The actual nature of charge transport would depend on the relative mobility of these two different kinds of carriers as demonstrated by the fact that the electronic conductivity of PEDOT/V_2O_5 is 10^2 times higher than that of pristine V_2O_5. In all samples, the conductivity is almost exclusively electronic and increases with an increase in the temperature as seen in most intercalated compounds and conjugated polymers.[6−14] For similar PEDOT/V_2O_5 samples synthesized by microwave irradiation for different time intervals, room temperature conductivity varies from 10^{-3} to 10^{-4} S cm^{-1}. In this case the increase in conductivity is probably due to a continued process of growth of the polymer network between the V_2O_5 layers (see Table 1).

Electrochemical Studies. Electrochemical measurements were performed based on the cell configuration of the Li|1 M $LiClO_4$ in EC/DMC (1:1 v/v)|PEDOT/V_2O_5 nanocomposite electrode. Figure 5 shows comparative cyclic voltammograms of (a) crystalline V_2O_5 and (b) the PEDOT/V_2O_5 nanocomposite, illustrating a drastic change in electrochemical properties induced by the polymer insertion. During the first cathodic scan, from the open-circuit voltage to 2.2 V vs Li/Li^+, the crystalline V_2O_5 undergoes a well-known phase transformation and the stabilization occurs after the third cycle (Figure 5a). The irreversible shift in the cathodic peak from 2.65 V (first cathodic scan) to 2.82 V (third and following cathodic scans) suggests that the structural change is permanent as reported elsewhere.[32−35] This type of voltammogram of crystalline V_2O_5 is different from that of vanadium pentoxide xerogels $V_2O_5 \cdot nH_2O$ as reported by Livage and also Anaissi et al.[5,9] since amorphous xerogels are known to exhibit enhanced electrochemical behavior in terms of faradic yields and reversibility. Further, the weak interactions between the interlamellar layers allow fast insertion of Li^+ ions between the ribbons rather than that in the channels of crystalline vanadium pentoxide.[9] In contrast, for the PEDOT/V_2O_5 hybrids, there is no sign of any irreversible structural change (Figure 5b); however, the broad cathodic peak resembles that of 2D V_2O_5 compounds.[36−39] The broad and diffuse peak shape can, therefore, be correlated with the layer stacking derived by the polymer incorporation, as previously deduced from X-ray diffraction data.

Figure 6 demonstrates the potential vs capacity curves for the first two cycles carried out at a rate of 15 mA h g^{-1} in the voltage range of 2.0−4.4 V (vs Li^+/Li), corresponding to the uptake of ∼2 lithium atoms per V_2O_5 unit. The discharge profile of pristine V_2O_5 shows a distinct plateau due to structural

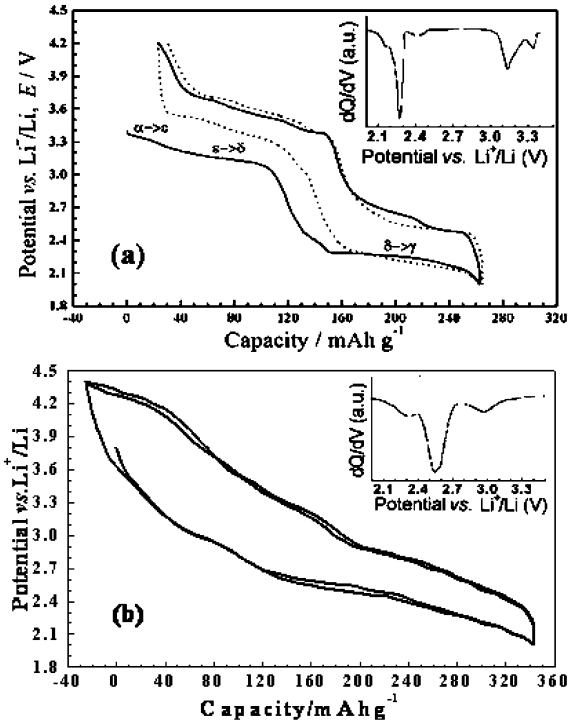

Figure 6. Potential vs capacity curves for the first two cycles of (a) pristine V_2O_5 and (b) the PEDOT/V_2O_5 nanocomposite prepared from direct microwave irradiation for 8 min. The insets show the corresponding differential capacity profiles of the first discharge. The potential range was set to 2.0−4.4 V vs Li, and the current density was fixed to 15 mA/g.

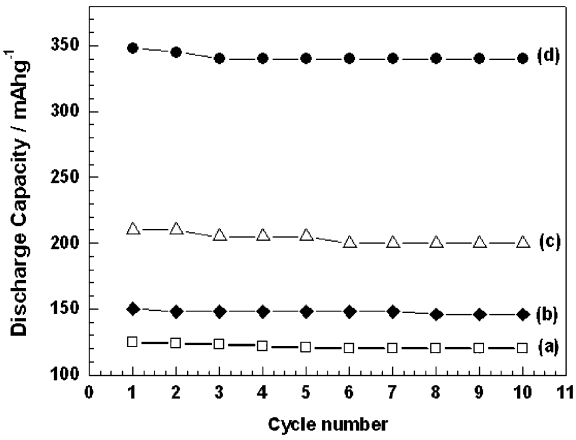

Figure 7. Evolution of the discharge capacity with the number of cycles for various cathode materials: (a) $Li_xMn_2O_4$, (b) Li_xCoO_2, and (c) $LiMn_xCo_{1-x}O_2$ compared with (d) PEDOT/V_2O_5. The potential range was set to 2.0−4.4 V for the PEDOT/V_2O_5 nanocomposite.

changes from α-V_2O_5 to ϵ-$Li_xV_2O_5$, to δ-$Li_xV_2O_5$, and then finally to γ-$Li_xV_2O_5$, resulting in a curve shape change in the second cycle. On the contrary, the potential decreases more smoothly down to ∼2.7 V for the nanocomposite, displaying a minor plateau around 2.5 V. A similar continuous decrease in potential has also been observed for the V_2O_5 xerogel, and for other conductive polymer/V_2O_5 nanocomposites, where the common structural feature is the enhanced separation of vanadium oxide layers due to the presence of interlayer molecules. It is worth mentioning that the PEDOT/V_2O_5 nanocomoposite reveals a larger capacity during the first charge than the first discharge. It can be attributed to the presence of V^{4+}, which could be easily oxidized by an electrochemical method, as already reported in the case of conductive polymer/V_2O_5 hybrids.[40,41] A more accurate inspection of the insertion voltage is accomplished by the analysis of differential capacity profiles of the first discharge. The sharp peaks of pristine V_2O_5 are typical traits of the phase transformations, while, on the contrary, the nanocomposite exhibits gross peaks. Interestingly, the PEDOT/V_2O_5 nanocomoposite delivers 350 mA h g^{-1} while the pristine V_2O_5 produces only 240 mA h g^{-1} in the second discharge at similar charge−discharge rates. The improved performance of the hybrid material is presumably due to the larger separation between vanadium oxide layers, leading to an enhanced "bidimensionality". Figure 7 shows the evolution of discharge capacity with cycle life for various commercially available cathode materials, such as $LiMn_2O_4$, $LiCoO_2$, and $LiMn_xCo_{1-x}O_2$ compared with our PEDOT/V_2O_5 nanocomposite. This comparative analysis clearly suggests that the polymer nanocomposite can act as a promising cathode material for high-energy-density rechargeable lithium microbatteries.

Conclusions

In conclusion, we have successfully demonstrated the feasibility of synthesizing a PEDOT/V_2O_5 hybrid nanocomposite for the first time by a unique, fast, and energy-efficient microwave technique. The selection of microwave irradiation plays a key role in significantly reducing the time for preparation (within 8 min) compared to that of conventional preparative strategies. The method is very attractive for large-scale production in view of the very short time involved for the synthesis. XRD and HRTEM suggested that the interlayer distance of crystalline V_2O_5 expands upon the incorporation of the polymer nanoribbons, while X-ray photoelectron spectra show the presence of both V^{4+}/V^{5+} species in the nanocomposite, also suggesting this reduced species V^{4+} in the V_2O_5 slabs due to oxidative polymerization. These results also confirm the redox intercalation process and charge transfer from the polymer to the V_2O_5 framework. The improved electrochemical performance, observed with the intercalation of conductive PEDOT macromolecules, is consistent with both the expansion of the interlayer distance and electronic conductivity of the vanadium oxide host. The origin of enhanced conductivity has also been investigated by EPR spectroscopy, which gives evidence for the two types of VO^{2+} complexes; that is, one is isolated and the other is nonisolated. Thus, the microwave-assisted intercalation of PEDOT in V_2O_5 produces a new functional nanocomposite which can act as a promising cathode material for high-energy-density rechargeable lithium batteries. This method of rapid synthesis of such remarkably efficient hybrid materials for rechargeable lithium batteries using microwave irradiation could be extended to other similar systems, providing new opportunities and challenges in the field of microwave synthesis.

Acknowledgment. A.V.M. thanks M/s. Bayer AG, Germany, and Mr. S. D. Joshi, Bayer India Ltd., Mumbai, for kindly providing the EDOT monomer, the late Dr. Subbanna, IISc, Bangalore, for HRTEM analysis, and Mr. Vijayaraj and Miss Priya, National Chemical Laboratory (NCL), Pune, for helping with the XRD and electrical conductivity measurements and also acknowledges Dr. S. Sivaram, Director, NCL, and Dr. B. K. Das, Executive Director, C-MET. This work was supported by the Ministry of Non-conventional Energy Sources & Ministry of Communication and Information Technology, Government of India.

References and Notes

(1) Iijima, S. *Nature* **1991**, *354*, 56.
(2) Spahr, M. E.; Bitterli, P. S.; Nesper, R.; Hass, O.; Novák, P. *J. Electrochem. Soc.* **1999**, *146*, 2780.

(3) Xia, Y.; Yang, P.; Sun, Y.; Wu, Y.; Mayers, B.; Gates, B.; Yin, Y.; Kim, F.; Yan, H. *Adv. Mater*. **2003**, *15*, 353.

(4) Wen, J. G.; Lao, J. Y.; Wang, D. Z.; Kyaw, T. M.; Foo, Y. L.; Ren, Z. F. *Chem. Phys. Lett*. **2003**, *372*, 717.

(5) Livage, J. *Chem. Mater*. **1991**, *3*, 578.

(6) Wu, C.-G.; DeGroot, D. C.; Marcy, H. O.; Schindler, J. L.; Kannewurf, C. R.; Liu. Y.-J.; Hirpo, W.; Kanatzidis, M. G. *Chem. Mater*. **1996**, *8*, 1992.

(7) Kerr, T. A.; Wu, H.; Nazar, L. F. *Chem. Mater*. **1996**, *8*, 2005.

(8) Leurox, F.; Goward, G.; Power, W. P.; Nazar, L. F. *J. Electrochem. Soc*. **1997**, *144*, 3886.

(9) Anaissi, F. J.; Demets, G. J. F.; Toma, H. E. *Electrochem. Commun*. **1999**, *1*, 332.

(10) Shouji, E.; Buttry, D. A. *Langmuir* **1999**, *15*, 669.

(11) Lira-Cantu, M.; Gomez-Romero, P. *J. Electrochem. Soc*. **1999**, *146*, 2029.

(12) Kuwabata, S.; Masui, S.; Tomiyori, H.; Yoneyama, H. *Electrochim. Acta* **2000**, *46*, 91.

(13) Gomez-Romero, P. *Adv. Mater*. **2001**, *13*, 163.

(14) Vadivel Murugan, A.; Kale, B. B.; Kwon, C.-W.; Campet, G.; Vijayamohanan, K. *J. Mater. Chem.* **2001**, *11*, 2470.

(15) Huguenin, F.; Torresi, R. M.; Buttry, D. A. *J. Electrochem. Soc*. **2002**, 149, A546.

(16) Vadivel Murugan, A.; Kwon, C.-W.; Campet, G.; Kale, B. B.; Maddanimath, T.; Vijayamohanan, K. *J. Power Sources* **2002**, *105*, 1.

(17) Kwon, C.-W.; Vadivel Murugan, A.; Campet, G.; Portier, J.; Kale, B. B.; Vijayamohanan, K.; Choy, J. H. *Electrochem. Commun*. **2002**, *4*, 384.

(18) Kwon, C.-W.; Poquet, A.; Mornet, S.; Campet, G.; Portier, J.; Vadivel Murugan, A.; Kale, B. B.; Vijayamohanan, K.; Choy, J. H. *Mater. Res. Soc. Symp. Proc*., **2002**, *726*, Q11.7.1.

(19) Ferreira, M.; Huguenin, F.; Zucolotto, V.; Pereira de Silva, J. E.; Cordoba de Torresi, S. I.; Temperini, M. LA.; Torresi, R. M.; Oliveira, O. N., Jr. *J. Phys. Chem. B* **2003**, *107*, 8351.

(20) Palchik, O.; Avivi; Pinkert, D.; Gedanken, A. *Nanostruct. Mater*. **1999**, *11*, 415, 20.

(21) Rao, K. J.; Vaidhyanathan, B.; Ganguli, M.; Ramakrishnan, P. A. *Chem. Mater*. **1999**, *11*, 882.

(22) Bhat, M. H.; Chakravarthy, B. P.; Ramakrishnan, P. A.; Levasseur, A.; Rao, K. J. *Bull. Mater. Sci.* **2000**, *23*, 461.

(23) Zhu, J.; Zhou, M.; Xu. J.; Liao, X. *Mater. Lett.* **2001**, *47*, 25.

(24) Vadivel Murugan, A.; Sonawane, R. S.; Kale, B. B.; Apte, S. K.; Kulkarni, A. V. *Mater. Chem. Phys.* **2001**, *71*, 98.

(25) Watanabe, T.; Shimizu, A.; Inagaki, M. *J. Mater. Chem*. **1995**, *5*, 753.

(26) Inagaki, M.; Nakamura, T.; Shimizu, A. *J. Mater. Res.* **1998**, *13*, 896.

(27) Petkov, V.; Trikalitis, P. N.; Bozin, E. S.; Billinge, S. J. L.; Vogt, T.; Kanatzidis, M. J. *J. Am. Chem. Soc*. **2002**, *124*, 10157.

(28) Wagner, C. D.; Riggs, W. M.; Davis, L. E.; Moulder, J. F.; Muilenberg, G. E. *Handbook of X-ray photoelectron spectroscopy*; Perkin-Elmer Corp.: Eden Prairie, MN, 1979.

(29) Yeh, J. J.; Lindau, I. *At. Data Nucl. Data Tables* **1985**, *32*, 1.

(30) Pecquenard, B.; Gourier, D.; Baffier, N. *Solid State Ionics* **1995**, *78*, 287.

(31) Stallworth, P. E.; Johnson, F. S.; Greenbaum, S. G.; Passerini, S.; Flowers, J.; Smyrl, W.; Fontanella, J. J. *Solid State Ionics* **2002**, *146*, 43.

(32) Cocciantelli, J. M.; Broussely, M.; Doumerc, J. P.; Labat, J.; Pouchard, M. *J. Power Sources* **1991**, *34*, 103.

(33) Cocciantelli, J. M.; Ménétrier, M.; Delmas, C.; Doumerc, J. P.; Pouchard, M.; Broussely, M.; Labat, J. *Solid State Ionics* **1995**, *78*, 143.

(34) Tranchant, A.; Blengino, J. M.; Farcy, J.; Messina. *J. Electrochem. Soc.* **1992**, *139*, 1243.

(35) West, K.; Zachau-Christiansen, B.; Jacobsen, T.; Skaarup, S. *Solid State Ionics* **1995**, *76*, 12.

(36) Sato, Y.; Nomura, T.; Tanaka, H.; Kobayakawa, K. *J. Electrochem. Soc*. **1991**, *138*, L37.

(37) Sato, Y.; Asada, T.; Tokugawa, H.; Kobayakawa, K. *J. Power Sources* **1997**, *68*, 674.

(38) Sato, Y.; Matsueda, T.; Tokugawa, H.; Kobayawa, K. *Chem. Lett*. **1993**, 901.

(39) Ugaji, M.; Hibino, M.; Kudo, T. *J. Electrochem. Soc.* **1995**, *142*, 3664.

(40) Goward, G. R.; Leroux, F.; Nazar, L. F. *Electrochim. Acta* **1998**, *43*, 1307.

(41) Bullot, J.; Cordier, P.; Gallais, O.; Gauthier, M.; Babonneau, F. *J. Non-Cryst. Solids* **1984**, *68*, 135.